Automated inspection of gaps on the automobile production line through stereo vision and specular reflection

Dimitrios Kosmopoulos , Theodora Varvarigou

Abstract

One of the most difficult tasks in the later stages of automobile assembly is the dimensional inspection of the gaps between the car body and the various panels fitted on it (doors, motor-hood, etc.). The employment of an automatic gap-measuring system would reduce the costs significantly and would offer high flexibility. However, this task is still performed by humans and only a few — still experimental — automatic systems have been reported. In this paper, we introduce a system for automated gap inspection that employs computer vision. It is capable of measuring the lateral and the range dimension of the gap (width and flush, correspondingly). The measurement installation consists of two calibrated stereo cameras and two infrared LED lamps, used for highlighting the edges of the gap through specular reflection. The gap is measured as the 3D distance between the highlighted edges. This method has significant advantages against the laser-based, gap-measuring systems, mainly due to its color independency. Our approach has been analytically described in 2D and extensively evaluated using synthetic as well as real gaps. The results obtained verify its robustness and its applicability in an industrial environment.

Keywords: Automated visual inspection; Specular reflection; Gap measurement

1. Introduction

The inspection of produced cars is a significant part of the manufacturing process that includes the dimensional inspection of the openings (gaps) between the surface parts of the vehicle. Gap inspection receives a great deal of attention during the assembly process due to the fact that the related faults are visible, cause bad insulation of the passengers' cabin and unpleasant noise at high speed. Many manufacturers desire 100% inspection to enhance their competitiveness. However, the gap-measuring task in the automobile industry has been automated at a very slow pace and it is still performed by humans. Using humans for 100% inspection requires considerable manpower that significantly increases the costs and the time for inspection.

In the aerospace industry, Chalupnik et al. [1] and Sarr and Jurick [2] have reported some techniques for measuring the width of a gap. In the automobile industry, the problem of measuring gaps has been addressed since the early 1980s. The methods that are used for measuring gap width or flush (lateral and range dimension, correspondingly) can be categorized as follows:

- the mechanical methods use a deformable probe that is fitted into the gap and reveals its width or flush;

- the ultrasonic methods find the width of a gap by measuring the time needed for a high frequency signal to propagate across it;
- the electrical methods find the width by measuring electrical characteristics of the gap such as capacitance.

The above techniques cannot be automated and, therefore, they are not appropriate for 100% on-line inspection. The task of measuring gaps with the above methods is tedious, time-consuming and results in high labor costs. Furthermore, most of those methods provide low precision, subjective results and many errors are disregarded due to time limitations. Moreover, the mechanical measuring devices become easily worn out (and as a result inaccurate) and can harm the car's surface through contact. An additional problem is that the manual measurements are difficult to record. All these problems necessitate the installation of an automated inspection system, which will be able to measure continuously large vehicle volumes precisely and consistently.

An optical visual gap inspection system has significant advantages compared to the non-visual methods. The task can be executed very fast with no human interference and a constant, consistent, 100% monitoring of the production can be achieved. The accuracy of the measurement is high and there is no risk of damaging the product since the measurement is non-contact. The measurements can be automatically stored into databases and by statistical evaluation weak points in the production process can be identified and corrected as they occur, saving time, energy and labor.

The literature regarding automated gap inspection systems is rather limited. Many inspection systems have not even been reported in the literature probably due to proprietary considerations. Potentially most methods that supply range data with high accuracy could be used for measuring gaps. Many publications have described gap-measuring systems for robot arc welding tasks. Most of them use range sensors, which are based on active triangulation, e.g. [3–5]. In these examples, a light projector emits a plane of laser light, which is projected as a bright stripe on a direction transverse to the gap. A camera can identify the position of the stripe in 3D space if the relative position and orientation between the camera and the light projector are known. Gap dimensions can then be obtained by the produced range data. The laser beam can be replaced by one or more light stripes or patterns as mentioned by Pritschow and Horn [6], with a reported accuracy of about 0.1 mm.

Many companies have dealt with the problem of automated visual inspection of gaps. ''Third Dimension Software Ltd.'' [7] has implemented a device called ''Gap Gun'', which projects a laser stripe on the gap and a camera acquires range data based on the principle of active triangulation. ''Oxford Sensor Technology Ltd.'' [8] uses the ''QuickScan Profile Measurement Sensor'' for a variety of measuring tasks, one of which has to do with gaps. The same triangulation principle is used but in this case a circle instead of a stripe is projected, so that the orientation angles of the measured surfaces can be additionally obtained. The resolution of the above systems varies from 0.025 to 0.35 mm, depending on the configuration.

The laser-based sensors are difficult to use when the target objects have a variety of colors. In this case, the intensity of the laser beam has to be adjusted to the color of the target that is measured, otherwise the projected beam will be invisible on dark colors or too bright on highly reflective ones. In an environment such as the assembly line, where the color of the measured object is not known a priori, additional systems for color recognition have to be installed. The problem becomes even greater when the parts that constitute the gap are not uniformly colored. Furthermore, a laser cannot measure transparent materials such as glass and, thus, gaps formed by the windscreen or the headlights are not measurable using laser-based sensors. Moreover, the laser-based sensors need many camera cycles in order to scan a complete gap profile with the same beam. This is a disadvantage when the vehicles to be measured are on fast conveyors and there is no time for a complete scan.

The company ''Oxford Sensor Technology Ltd.'' [9] has also developed the ''Specular Reflection Sensor'', which was designed for automatic windscreen insertion in car assembly. It uses diffuse illumination (one LED lamp) and two coplanar line cameras to identify the reflections on rounded edges. The line cameras offer shorter frame cycles and higher resolution than the CCD cameras (the system has an accuracy better than 0.1 mm). On the other hand, for

measuring a gap section the device has to be moved mechanically over the gap in order to scan it that results in many camera cycles. Additionally, due to the coplanar placement of the cameras the flush cannot be measured as accurately as the gap, probably due to the application requirements. Another problem of this approach is that the device has to be close to the nominal standoff distance; otherwise the measurement will be inaccurate. The nominal distance cannot be much >250 mm due to lighting considerations and by using only one light source the device can be applied to limited gap geometries.

The next section describes how we have used the specular reflection to measure gaps with a pair of cameras. The system configuration, the employed algorithms and the properties of specular reflection are examined. Section 3 presents several experimental results. The final section summarizes the characteristics of our approach and describes current and future work.

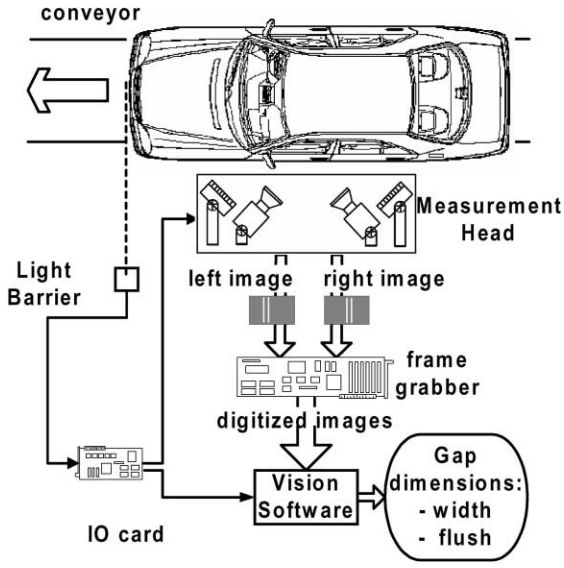

Fig. 1. The principal structure of a gap-measuring system. A light barrier triggers the measurement head to acquire images, whenever a vehicle appears and the vision software extracts from the grabbed images the dimensions of the gap.

2. Gap inspection with cameras

2.1. Overview

This paper proposes a new system for automated visual inspection of gaps on vehicles. An overview of the system is illustrated in Fig. 1. The system consists of two cameras for stereo vision and two infra red LED lamps for highlighting the gap. A light barrier triggers the measurement and the vision software extracts from the images the dimensions of the gap. Our system overcomes the limitations of the methods described in Section 1. Its accuracy is also about 0.1 mm, which is sufficient for gap inspection [7–9].

In stereo vision, the correspondence problem is inherently under-constrained and, therefore, constraints have to be imposed by making assumptions regarding scene reflectance and structure [10]. However, in the presence of specular reflection, these assumptions fail, since highlights are assumed to be real scene features [11] and, therefore, many methods have been developed to eliminate any virtual features resulting from specular reflection (e.g. [12]). In our approach, these highlights are desirable and we treat them as real features to identify a gap. Generally, the position of highlights in the image is viewpoint-dependent but for a small radius of curvature of the profile, as in this application, the highlights remain almost at the same position [13] and, thus, they can be used for measurement. In Section 2.3, we show how we can alleviate the slight movement of the highlights.

The gaps that we have measured are located (a) between two doors, (b) between the motor-hood and the splashboard, (c) between the trunk and the splashboard and (d) between the door and the roof. In all these cases, the edges of the gap constituents are not perfectly sharp but have a certain curvature, whose radius can be up to a few millimeters. This enables us to highlight the gap faces and make them recognizable by a vision system (Fig. 2). We have successfully tested the method also on gaps constituted of transparent edges such as motor hood-headlight and windscreen-car body (case in which the laser sensors cannot be applied). Our method depends on the geometry of the gap and not on its color. Thus, the great variety of colors that is met on the assembly line does not influence the measurements. In addition to it, by employing area CCD cameras the gap profile can be extracted in only one camera cycle and independently

Fig. 2. A gap on the outer surface of a vehicle, which is highlighted for measurement purposes.

of the vehicle's speed. Thus, there is no need to stop the conveyor in order to measure and, hence, the production is not interrupted.

Our system has advantages also with regards to the ''Specular Reflection Sensor''. Since the direct illumination is used (which guarantees reflections of the maximum brightness) the measurement hardware can be installed at distances as large as 1 m, which complies with the safety regulations for measuring on the assembly line. The use of two lamps instead of one gives us the flexibility to create the appropriate reflections on gaps of various geometries. Our system can perform measurements even if the vehicle is displaced several centimeters from its nominal standoff position.

2.2. System configuration

Camera parameters and illumination are very important in visual inspection tasks. The methodology used for defining them falls into the area of sensor planning as reported by Tarabanis et al. [14]. In our system, we have used this methodology in order to quantify the relationship between the gaps to be viewed and the system components in a model-based way.

In the related literature concerning camera planning, a series of requirements have been identified that affect the camera placement as reported by Cowan and Kovesi [15], Mason and Grün [16] and Tarabanis et al. [14,17]. The resolution constraint provides an upper bound on the distance between the camera and the gap. In our case, we can position the cameras so that the lines appear always vertical in the image, in order to increase the resolution as mentioned by Cowan and Kovesi [15]. The focus constraint determines the region of viewpoints so that the observed gap is always in focus. In this application, there is some uncertainty in the position of the gap, so the depth of field of the cameras must cover the whole volume of interest. The constraints regarding the field of view and the visibility, which require that the gaps to be observed must lie completely within the camera field of view and must be visible, are covered by the focus constraint. The view angle constraint determines the angle from which we can measure in the x- and y-coordinate axes with a homogeneous precision (as explained by Mason and Grün [16]. The working environment imposes the additional constraint of the minimum vertical distance of the cameras to the vehicle surface, due to safety considerations. The placement of the cameras in our system is compatible with the above requirements and is illustrated in Fig. 3. C_1, C_2 are the perspectivity centers of the cameras and $(C_1; \boldsymbol{x}_1, \boldsymbol{y}_1, \boldsymbol{z}_1)$, $(C_2; \boldsymbol{x}_2, \boldsymbol{y}_2, \boldsymbol{z}_2)$ are the coordinate systems of the cameras. We name $\boldsymbol{n}_1, \boldsymbol{n}_2$ the normal vectors to the planes defined by the outer surfaces of the parts that constitute the gap. We assume that $\boldsymbol{n}_1 = \boldsymbol{n}_2$ and we place the cameras so that $\boldsymbol{z}_1$, $\boldsymbol{z}_2$ lie on the same plane p,

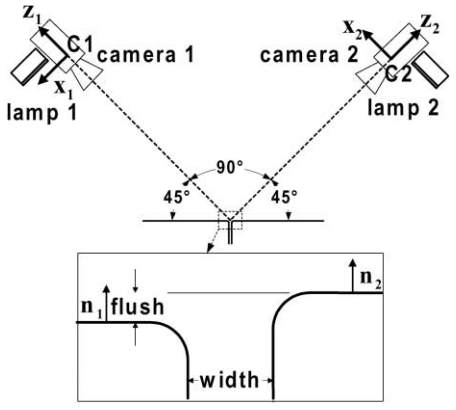

Fig. 3. The optimal system configuration, which requires a symmetric angle of 45° between the cameras and similar positioning for the lamps. The quantities to be measured (width and flush) appear magnified.

which is vertical to the surfaces of $\boldsymbol{n}_1$, $\boldsymbol{n}_2$. The gap must be centered in the image of each camera. The cameras are placed so that their z-axes have a relative angle of $+45$ and -45° to $\boldsymbol{n}_1$, $\boldsymbol{n}_2$.

The next step, which is *Illumination planning*, is to determine the illumination and the related constraints to be considered (illumination or radiometric constraints, reported by Tarabanis et al.) [14]. The feature to be detected must be visible by the light source, the image irradiance from the feature must be within the dynamic range of the camera and the contrast of the edges must be high. The faces of the gaps that we intend to measure have a certain curvature, whose radius can be up to a few millimetres and, thus, we regard the gap faces as cylindrical convex mirrors. The light is reflected on the gap surface and if we use appropriately designed lamps we can highlight the gap. The behavior of the highlights (bright lines) can be described by the ray tracing equations, which are well known from the field of optics and computer graphics. It is easier to solve the problem in two-dimensions and then to extend the conclusions to 3D. The 2D projection of the cylindrical mirror is a circular mirror and the bright line becomes a bright point (highlight point). The law of specular reflection gives the angle of the highlight point θ:

$$\theta = \frac{\phi + \omega}{2} \tag{1}$$

where the angles ϕ, ω correspond to the light source S and the viewpoint C (Fig. 4). The illumination has to

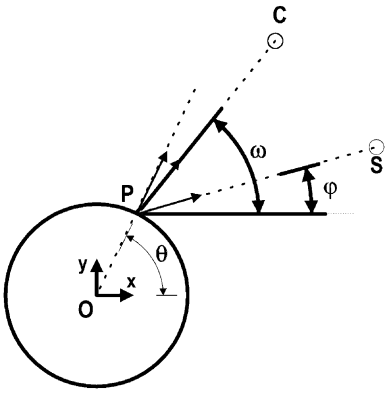

Fig. 4. Specular reflection on a circular mirror: the highlight P, the viewpoint C, the light source S, and the corresponding angles θ, ω, φ.

be such that both cameras see one bright line on each gap face. Since the cameras are symmetrically positioned with respect to the gap, we infer that the illumination should also be symmetrical. A possible solution would be a lamp located on the gap symmetry axis, since the symmetry is maintained and a great amount of light is reflected. Unfortunately, in this configuration the whole lamp is mirrored on the surfaces and not just two thin bright lines. Due to the fact that the only symmetric solution with one lamp is rejected, we have to use two lamps located as far as possible from the symmetry axis in order to avoid the above effect. By increasing the distance of a lamp from the symmetry axis a bright line appears on the opposite gap face (in both cameras). We expect no bright line on the nearest one, due to the fact that the incident beam is tangential to its surface. The above constraints are satisfied if we put the first lamp close to the camera, as illustrated in Fig. 3. The second lamp must be installed symmetrically. As explained in the next section, the measured dimensions of the gap differ from the actual ones and this is illustrated in Fig. 3.

In three-dimensions, we do not have spot light sources but linear ones vertical to the aforementioned plane p. The cameras see lines, which are also vertical to p, since the image planes are vertical to p. The length of the bright line is proportional to the length of the lamp (it is obvious that the long side of the lamp should be positioned parallel to the edges that have to be highlighted). The width of the lamp affects the width of the bright lines especially if the curvature is big.

2.3. Measurements

In this section, we will describe the principles behind the measurement system. The measurement technique is presented and we will see how we can obtain the actual gap dimensions from the system measurements. Furthermore, we will show that the measurements are affected when the gap is displaced from its nominal standoff position and we will see how we can compensate for this effect.

2.3.1. Gap extraction method

For *measurement in 2D*, the identification of the gap in each image is performed with subpixel accuracy

using the concept of the active contour followers (snakes), which was introduced by Kass et al. [18]. More specifically, we seek to minimize the quantity:

$$e(\boldsymbol{V}, \lambda) = \lambda \cdot E_{\text{int}}(\boldsymbol{V}) + (1 - \lambda) \cdot E_{\text{ext}}(\boldsymbol{V}) \tag{2}$$

where vector $\boldsymbol{V}$ represents the position of the snake elements, E_{int} is the internal energy of the snake, E_{ext} the energy associated with the force that attracts the snake towards the image contour and λ a factor between 0 and 1 as mentioned by Lai [19]. We know a priori that the gap will appear almost vertical in the image (due to the used configuration of cameras and lamps) and within a limited region (region of interest: ROI). By examining the intensity profile of a horizontal scanline that crosses the ROI we are able to locate the x-position of the bright lines in the image. The intersections of the scanline with the bright lines define the initial positions of the vertical, line-shaped snakes. The initial position of the snakes is very close to the actual position of the lines and, therefore, the snake converges in just 1 cycle. The line is easily obtained from the snake points with Hough transformation.

The error of the contour extractor may affect significantly the measurement and, therefore, high image quality and good snake parameterization are required. The rules applied for camera and illumination planning provide us with good resolution for width and flush and yield sharp and bright lines. As far as the snake is concerned, we were able to reduce the noise by choosing a large value for factor λ ($\lambda \approx 0.8$) as reported by Lai [19] since we only search for lines and we are not interested in detecting big curvatures. Using subpixel resolution and small spacing between the snake elements further enhances the accuracy.

For *measurement in 3D*, we have used the algorithm introduced by Tsai [20] and improved by Lenz and Tsai [21], to calculate the intrinsic and extrinsic parameters of the cameras (camera calibration) using a pattern of 209 coplanar circles. From the intrinsic and the extrinsic parameters and the 2D lines in both images we compute the 3D lines, as reported by Hager [22]. For the calculation of the width, we project the 3D lines onto the xy plane of the world coordinate system, which was defined during the calibration. Similarly, the flush is obtained by projecting the 3D lines on the xz plane of the world coordinate system. The width and the flush are extrapolated from the distance between the projected lines.

2.3.2. Measured and actual gap

The spatial position of the bright lines does not give directly the gap dimensions because it is viewpoint-dependent. Therefore, when the gap is displaced from its nominal standoff position the measurements change. Thus, the measured gap differs from the actual gap. In Fig. 4, the position of the highlight-point P in the coordinate system $(\mathrm{O}; \boldsymbol{x}, \boldsymbol{y})$ using (1) is the following:

$$\boldsymbol{r}_{\mathrm{P}} = (x_{\mathrm{P}}, y_{\mathrm{P}}) = \left(R \cos \frac{\phi + \omega}{2}, R \sin \frac{\phi + \omega}{2} \right) \tag{3}$$

The angles φ and ω are given by:

$$\begin{aligned} \varphi &= \arctan(x_{\mathrm{C}} - R\cos\theta,\, y_{\mathrm{C}} - R\sin\theta) \\ &\cong \arctan(x_{\mathrm{C}}, y_{\mathrm{C}}) \end{aligned} \tag{4}$$

$$\begin{aligned} \omega &= \arctan(x_{\mathrm{S}} - R\cos\theta,\, y_{\mathrm{S}} - R\cos\theta) \\ &\cong \arctan(x_{\mathrm{S}}, y_{\mathrm{S}}) \end{aligned} \tag{5}$$

The above approximation is made because in our case $R \leq 3$ mm, x_{C}, y_{C}, x_{S}, $y_{\mathrm{S}} \cong 500$ mm and the error in the calculation of θ is about 0.001%. Thus, from (3) to (5) we calculate:

$$\begin{aligned} \boldsymbol{r}_{\mathrm{P}} = \Bigg(& R \cos \frac{\arctan(x_{\mathrm{C}}, y_{\mathrm{C}}) + \arctan(x_{\mathrm{S}}, y_{\mathrm{S}})}{2}, \\ & R \sin \frac{\arctan(x_{\mathrm{C}}, y_{\mathrm{C}}) + \arctan(x_{\mathrm{S}}, y_{\mathrm{S}})}{2} \Bigg) \end{aligned} \tag{6}$$

In Fig. 5, C_1, C_2 denote the cameras and S_1, S_2 the point sources of light. As it is evident from Fig. 5, the highlight points seen by each camera are different and this complicates the problem. Camera 1 sees the highlights P_1, P_3 and camera 2 sees the highlights P_2, P_4. This happens due to the fact that Eq. (1) yields different solutions for different positions of the cameras when the camera angle ω changes. Point P_1 is matched with P_2 and P_3 with P_4. The reconstruction supplies the points P_{12} and P_{34}, correspondingly, which are obtained by the intersection of the extensions of the camera beams that go through the highlight points P_1, P_2 and P_3, P_4, correspondingly.

In Fig. 5, O_{L} and O_{R} denote the curvature centers on the left and right edge of the gap, which are the origins of the corresponding coordinate systems. For both

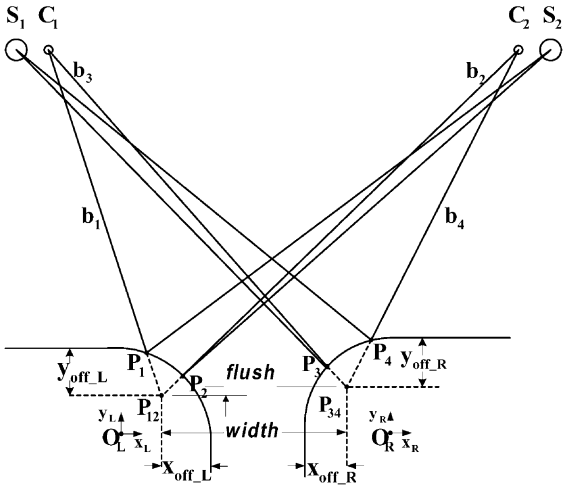

Fig. 5. Measuring a gap in two dimensions: the cameras C_1, and C_2 see the highlight points P_1, P_3 and P_2, P_4, respectively, which are created by the lamps S_1, S_2; the system reconstructs the points P_{12} and P_{34}, from which the width and flush are measured.

coordinate systems the x-axis is parallel to the width direction and the y-axis is parallel to the flush direction. The width and flush are measured as the difference in the x- and y-coordinates of P_{12} and P_{34}. In the coordinate system $(O_L; \boldsymbol{x}_L, \boldsymbol{y}_L)$ we define the points P_i, C_i, S_i with $\boldsymbol{r}_{P_i} = (x_{P_i}, y_{P_i})$, $\boldsymbol{r}_{C_i} = (x_{C_i}, y_{C_i})$, $\boldsymbol{r}_{S_i} = (x_{S_i}, y_{S_i})$ where $i = 1, 2$. The coordinates of the reconstructed point P_{12} are given by $\boldsymbol{r}_{P_{12}} = (x_{P_{12}}, y_{P_{12}})$. The beam b_i goes through the points C_i, P_i, so the following equations apply ($i = 1, 2$):

$$b_i : y = \frac{y_{C_i} - y_{P_i}}{x_{C_i} - x_{P_i}} x + \frac{-x_{P_i} y_{C_i} + x_{C_i} y_{P_i}}{x_{C_i} - x_{P_i}} \tag{7}$$

The point P_{12} is calculated as the intersection of the beams b_1 and b_2 and it is obtained by solving (7) for the unknowns x and y:

$$x_{P_{12}} = \frac{(x_{C_2}x_{P_1} - x_{P_1}x_{P_2})y_{C_1} + (x_{P_1}x_{P_2} - x_{C_1}x_{P_2})y_{C_2} + (x_{C_1}x_{P_2} - x_{C_1}x_{C_2})y_{P_1} + (x_{C_1}x_{C_2} - x_{C_2}x_{P_1})y_{P_2}}{f(x_{P_1}, x_{P_2}, x_{C_1}, x_{C_2}, x_{P_1}, y_{P_2}, y_{C_1}, y_{C_2})} \tag{8a}$$

$$y_{P_{12}} = \frac{(x_{P_1} - x_{P_2})y_{C_1}y_{C_2} + (x_{P_2} - x_{C_1})y_{C_2}y_{P_1} + (x_{C_2} - x_{P_1})y_{C_1}y_{P_2} + (x_{C_1} - x_{C_2})y_{P_1}y_{P_2}}{f(x_{P_1}, x_{P_2}, x_{C_1}, x_{C_2}, x_{P_1}, y_{P_2}, y_{C_1}, y_{C_2})} \tag{8b}$$

where $f = (x_{C_2} - x_{P_2})y_{C_1} + (x_{P_1} - x_{C_1})y_{C_2} + (x_{P_2} - x_{C_2})y_{P_1} + (x_{C_1} - x_{P_1})y_{P_2}$.

The point P_i with $\boldsymbol{r}_{P_i} = (x_{P_i}, y_{P_i})$ (where $i = 1, 2$) is calculated if we use (6):

$$\boldsymbol{r}_{P_i}\left(R\cos\frac{\arctan(x_{C_i}, y_{C_i}) + \arctan(x_{S_2}, y_{S_2})}{2}, \right.$$
$$\left. R\sin\frac{\arctan(x_{C_i}, y_{C_i}) + \arctan(x_{S_2}, y_{S_2})}{2} \right) \tag{9}$$

For real gap dimensions, the offset vector that transforms the measured to the actual gap dimensions, if subtracted from the measurements' vector, is calculated from the coordinates of P_{12}, P_{34} as follows. If we apply $x_{P_1}, x_{P_2}, y_{P_1}, y_{P_2}$ from (9) to (8a–b), we obtain the coordinates of P_{12} in $(O_L; \boldsymbol{x}_L, \boldsymbol{y}_L)$. The coordinates of P_{34} in $(O_R; \boldsymbol{x}_R, \boldsymbol{y}_R)$ are obtained in a similar way. The actual width is defined as the x-distance between the point $(R, 0)$ in $(O_L; \boldsymbol{x}_L, \boldsymbol{y}_L)$ and the point $(-R, 0)$ in $(O_R; \boldsymbol{x}_R, \boldsymbol{y}_R)$. Similarly, the flush is the y-distance between the point $(0, R)$ in $(O_L; \boldsymbol{x}_L, \boldsymbol{y}_L)$ and the point $(0, R)$ in $(O_R; \boldsymbol{x}_R, \boldsymbol{y}_R)$. We define as x_{off_L},y_{off_L}, x_{off_R},y_{off_R} the positive offsets in x- and y-direction on the left and right gap face so that

$$x_{off\_L} + x_{P_{12}} = y_{off\_L} + y_{P_{12}} = R \tag{10a}$$

$$x_{off\_R} - x_{P_{34}} = y_{off\_R} + y_{P_{34}} = R \tag{10b}$$

(see Fig. 5) where $\boldsymbol{r}_{P_{12}} = (x_{P_{12}}, y_{P_{12}})$, $\boldsymbol{r}_{P_{34}} = (x_{P_{34}}, y_{P_{34}})$ are the coordinates of P_{12} in $(O_L; \boldsymbol{x}_L, \boldsymbol{y}_L)$ and the coordinates of P_{34} in $(O_R; \boldsymbol{x}_R, \boldsymbol{y}_R)$, correspondingly. Then we have:

$$x_{off} = x_{off\_L} + x_{off\_R} = 2R - x_{P_{12}} - x_{P_{34}} \tag{11a}$$

$$y_{off} = y_{off\_L} - y_{off\_R} = y_{P_{12}} - y_{P_{34}} \tag{11b}$$

Thus, by subtracting the offset vector $\boldsymbol{r}_{off} = (x_{off}, y_{off})$ from the measured vector $\boldsymbol{r}_{meas} = (\text{width}, \text{flush})$ we transform the measured to the actual gap dimensions. The radius R that is needed for the above calculations is found in the CAD data of the produced parts.

A deviation of 0.1 mm from the nominal radius can introduce an error of about 0.015 mm to the above

results. The position of the cameras is found by the calibration algorithm with very high accuracy ($\approx$1 mm) so the introduced error is negligible. On the contrary the lamps' position is measured manually, with a precision of about 1 cm. This introduces an error smaller than 0.05 mm to the calculation of x_{off}, y_{off}.

Now we are going to calculate how the measurement is affected if the gap is displaced in x- and y-direction. We will calculate the change in the position of P_{12} in $(O_L; \boldsymbol{x}_L, \boldsymbol{y}_L)$ and similar equations will apply for P_{34} in $(O_R; \boldsymbol{x}_R, \boldsymbol{y}_R)$. If the gap is displaced then $\boldsymbol{r}_{P_i}$, $\boldsymbol{r}_{C_i}$ and $\boldsymbol{r}_{S_i}$ will change too and, thus, the measured $\boldsymbol{r}_{P_{12}}$ changes according to $\mathrm{d}\boldsymbol{r}_{P_{12}} = (\mathrm{d}x_{P_{12}}, \mathrm{d}y_{P_{12}})$, where:

$$\mathrm{d}x_{P_{12}} = \sum_{i=1}^{2}\left[\frac{\partial x_{P_{12}}}{\partial x_{C_i}}\,\mathrm{d}x_{C_i} + \frac{\partial x_{P_{12}}}{\partial x_{P_i}}\,\mathrm{d}x_{P_i} + \frac{\partial x_{P_{12}}}{\partial y_{C_i}}\,\mathrm{d}y_{C_i} + \frac{\partial x_{P_{12}}}{\partial y_{P_i}}\,\mathrm{d}y_{P_i}\right] \tag{12a}$$

$$\mathrm{d}y_{P_{12}} = \sum_{i=1}^{2}\left[\frac{\partial y_{P_{12}}}{\partial x_{C_i}}\,\mathrm{d}x_{C_i} + \frac{\partial y_{P_{12}}}{\partial x_{P_i}}\,\mathrm{d}x_{P_i} + \frac{\partial y_{P_{12}}}{\partial y_{C_i}}\,\mathrm{d}y_{C_i} + \frac{\partial y_{P_{12}}}{\partial y_{P_i}}\,\mathrm{d}y_{P_i}\right] \tag{12b}$$

All the partial derivatives are calculated from (8a–b). The vector $\mathrm{d}\boldsymbol{r}_{P_i} = (\mathrm{d}x_{P_i}, \mathrm{d}y_{P_i})$ $(i = 1, 2)$, whose coordinates are used in (12a–b) is calculated by differentiating (9) as follows:

$$\mathrm{d}x_{P_i} = \frac{\partial x_{P_i}}{\partial x_{C_i}}\,\mathrm{d}x_{C_i} + \frac{\partial x_{P_i}}{\partial x_{S_2}}\,\mathrm{d}x_{S_2} + \frac{\partial x_{P_i}}{\partial y_{C_i}}\,\mathrm{d}y_{C_i} + \frac{\partial x_{P_i}}{\partial y_{S_2}}\,\mathrm{d}y_{S_2} \tag{13a}$$

$$\mathrm{d}y_{P_i} = \frac{\partial y_{P_i}}{\partial x_{C_i}}\,\mathrm{d}x_{C_i} + \frac{\partial y_{P_i}}{\partial x_{S_2}}\,\mathrm{d}x_{S_2} + \frac{\partial y_{P_i}}{\partial y_{C_i}}\,\mathrm{d}y_{C_i} + \frac{\partial y_{P_i}}{\partial y_{S_2}}\,\mathrm{d}y_{S_2} \tag{13b}$$

By replacing $\mathrm{d}x_{P_i}, \mathrm{d}y_{P_i}$ to (12a–b), we have managed to express the $\mathrm{d}x_{P_{12}}$, $\mathrm{d}y_{P_{12}}$ as a function of $\mathrm{d}\boldsymbol{r}_{C_1} = (\mathrm{d}x_{C_1}, \mathrm{d}y_{C_1})$, $\mathrm{d}\boldsymbol{r}_{C_2} = (\mathrm{d}x_{C_2}, \mathrm{d}y_{C_2})$, $\mathrm{d}\boldsymbol{r}_{S_2} = (\mathrm{d}x_{S_2}, \mathrm{d}y_{S_2})$. If the gap is displaced from its zero position and the translation vector is $\mathrm{d}\boldsymbol{r} = (\mathrm{d}x, \mathrm{d}y)$ then:

$$\mathrm{d}\boldsymbol{r} = \mathrm{d}\boldsymbol{r}_{C_1} = \mathrm{d}\boldsymbol{r}_{C_2} = \mathrm{d}\boldsymbol{r}_{S_2} \tag{14}$$

Thus, we have managed to express the change in the position of the highlight point $\mathrm{d}\boldsymbol{r}_{P_{12}}$ as a function of the gap displacement from the nominal standoff position $\mathrm{d}\boldsymbol{r}$.

Given the displacement vector $\mathrm{d}\boldsymbol{r}$, in order to find the position $\boldsymbol{r}_{P_{34}}$ and the change $\boldsymbol{r}_{P_{34}}$ in the highlight position of P_{34} we have to replace in the Eqs. (7)–(9), (12) and (13), $\boldsymbol{r}_{S_2}$ with $\boldsymbol{r}_{S_1}$, $\boldsymbol{r}_{P_1}$ with $\boldsymbol{r}_{P_3}$ and $\boldsymbol{r}_{P_2}$ with $\boldsymbol{r}_{P_4}$. The coordinates are expressed in the $(O_R; \boldsymbol{x}_R, \boldsymbol{y}_R)$ coordinate system.

The change in the measurement $\mathrm{d}\boldsymbol{r}_{\text{meas}} = (\mathrm{d}(\text{width}), \mathrm{d}(\text{flush})$ is given by the equations:

$$\mathrm{d}(\text{width}) = \mathrm{d}x_{P_{34}} - \mathrm{d}x_{P_{12}} \tag{15a}$$

$$\mathrm{d}(\text{flush}) = \mathrm{d}y_{P_{12}} - \mathrm{d}y_{P_{34}} \tag{15b}$$

The sign for the calculation of d(width) is defined since we want $\mathrm{d}(\text{width}) > 0$ when the width increases and $\mathrm{d}(\text{width}) < 0$ when the width decreases. The sign for d(flush) is chosen arbitrarily. The quantities d(width), d(flush) have to be subtracted from the measurements in order to obtain the real dimensions of the gap.

After some algebraic manipulations the Eqs. (15a) and (15b) become as follows:

$$\mathrm{d}(\text{width}) = A(\boldsymbol{r}_{S_1}, \boldsymbol{r}_{S_2}, \boldsymbol{r}_{C_1}, \boldsymbol{r}_{C_2}, R)\mathrm{d}y \tag{16a}$$

$$\mathrm{d}(\text{flush}) = B(\boldsymbol{r}_{S_1}, \boldsymbol{r}_{S_2}, \boldsymbol{r}_{C_1}, \boldsymbol{r}_{C_2}, R)\mathrm{d}y \tag{16b}$$

Thus, the width measurement changes linearly when the gap is displaced along the y-axis with slope A, which is a function of $\boldsymbol{r}_{S_1}, \boldsymbol{r}_{S_2}, \boldsymbol{r}_{C_1}, \boldsymbol{r}_{C_2}$ and R. The flush measurement changes linearly in case of x-displacement with slope B, which is a function of the same parameters as A. The width and flush measurements remain unchanged when the gap is displaced along the x- and y-axis, correspondingly. For the symmetric system used in the experiments we calculated that $A \cong 0.00616$ and $B \cong -0.00321$ (Table 1).

3. Experimental results

3.1. Prototype system for measuring gaps

The prototype system that we used for our experiments consists of two off-the-shelf monochrome CCD cameras (TELI CS8420C-02) with COSMICAR lenses of 25 mm (the horizontal and vertical dimensions of the CCD elements are 0.0083 and 0.0086 mm, correspondingly), two infrared LED arrays with an active surface of 255 mm $\times$ 20 mm (custom designed), an RGB frame grabber card (Matrox Meteor 2MC),

Table 1
The theoretically calculated slopes regarding the measurement of width and flush for displacement of the gap along the x- and the y-axis

Displacement of x-axis		Displacement of y-axis	
Width slope	Flush slope (B)	Width slope (A)	Flush slope
0.00000	−0.00321	0.00616	0.00000

a power supply unit for the lamps and the cameras, a standard PC running the vision software (under Windows NT), the metal frame on which cameras and lamps were fixed, a shift table on which we clamped synthetic or reference gaps for off-line experiments (to move the gaps in x- and y-axis) and a light barrier (SICK) for triggering the measurement when measuring on the assembly line. The experimental installation for the off-line tests is illustrated in Fig. 6. For the on-line experiments we used the same equipment, with the addition of a light barrier (for triggering the measurement when the gap is in the cameras' field of view).

The control and data flow of the prototype softw are system is depicted in Fig. 7. The system is implemented as two processes, the Control and the Vision Process. Commands are issued and distributed through the Control Process, which is also used for the parameterization of the system. It consists of two threads, the ''User Interface'' and the ''Flow Controller'' (FC). The Vision Process undertakes every task that has to do with acquiring, distributing and processing images. Its task is to combine the extracted features from both cameras and to calculate the gap dimensions. It comprises of the threads ''Grab Control'', ''Feature Control1–2'', ''Feature Extraction1–2'' and ''Stereo Calculation''. ''Grab Control'' supplies the images, ''Feature Control'' controls the parameterized features, ''Feature Extraction'' finds the image coordinates of the gap and ''Stereo Calculation'' reconstructs the gap in 3D space and calculates the width and the flush. The ''Data Base'' maintains all the parameters of the system.

At this point we should mention that we parameterized the ''snakes'' that we used for the lines' identification to have a length that corresponds to about 1 cm. Our results were the average width and flush along this distance.

To set-up the system, we installed the cameras and the lamps as mentioned in Section 2.2. At this point, we should mention that the y-coordinates of the cameras and lamps resulted from the minimum allowed distance between the vehicle and the system components (workspace constraint). This configuration provided a resolution of about 5 pixels/mm, which is considered adequate for the purposes of

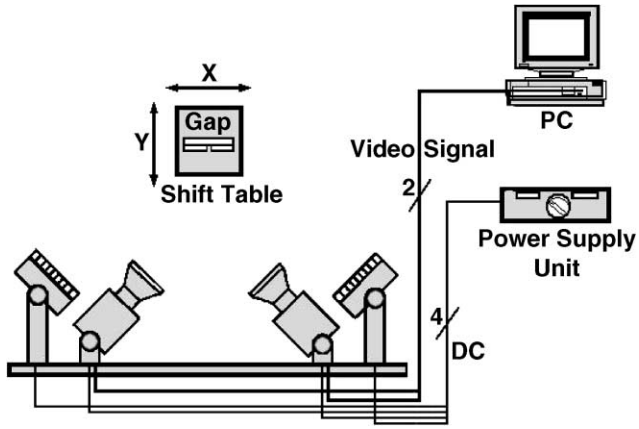

Fig. 6. Sketch of the off-line installation consisting of the pairs of cameras and lamps, the power supply, the host PC (with the vision software and hardware) and the target object (gap).

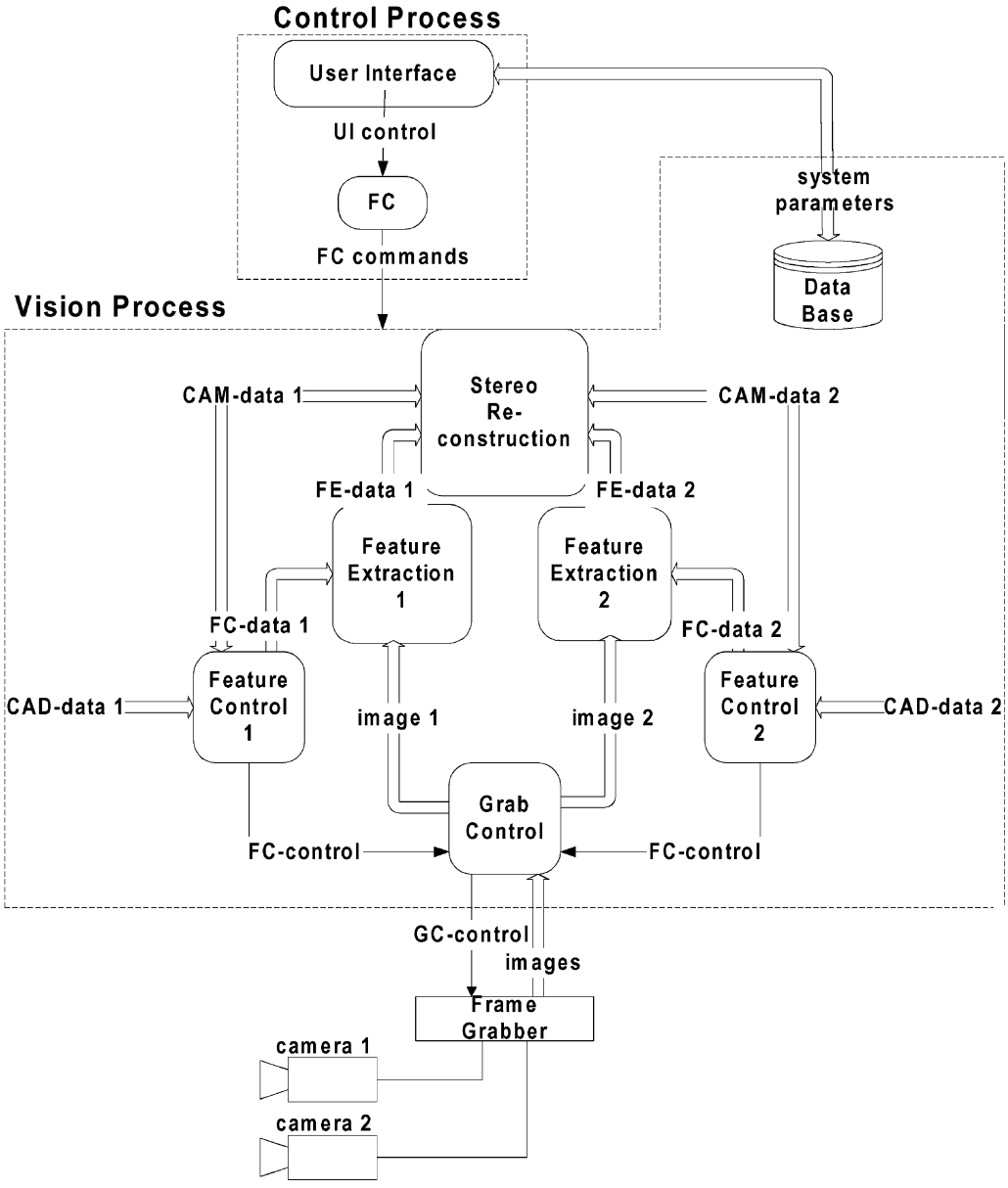

Fig. 7. The control and data flow of the prototype software system: *Feature Extraction* extracts from the acquired images the lines and then *Stereo Reconstruction* calculates the gap dimensions; the database stores permanently the system parameters and the user can issue high-level commands through the *User Interface*.

our prototype system, since we measured with sub-pixel accuracy. The field of view of the cameras covered an area of about 20 cm $\times$ 15 cm on the gap plane and the constraints related to focus, field-of-view and visibility were fulfilled. We calibrated the cameras using the pattern described in Section 2.3.1. For the off-line experiments we fixed the calibration plate on the shift table and we adjusted it at the zero position. We calibrated both cameras and then we replaced the calibration plate with the synthetic gap. For calibrating the on-line system we put the pattern on the gap of a moving vehicle and we

photographed it with the cameras. Then we used the acquired images to calibrate off-line.

3.2. Off-line experiments

In the off-line experiments, we verified the accuracy level of the measurement method and we studied how the measurement can be affected when the gap is displaced from its nominal standoff position. We measured initially a synthetic gap, consisting of a pair of bright lines etched on a metal plate to find the accuracy of the employed algorithms without the influence of the illumination. Then we measured a reference gap similar to those on the car-bodies, using the lamps, to estimate the errors coming from the illumination. We displaced the gap along the x- and along the y-axis within an area of 80 mm $\times$ 80 mm (on the assembly line: smaller than 40 mm $\times$ 40 mm). If the gap is displaced in both axes simultaneously the overall effect is calculated by combining the two effects.

3.2.1. Synthetic gap

In this experiment, we checked the measurement's accuracy for both width and flush, independently of the lamps' illumination. In other words we estimated the error that is attributed to the system configuration (employed algorithms and hardware). We used a synthetic gap, which had the form of a black metal plate, on which we etched with high accuracy two bright lines on parallel planes. These bright lines simulated the highlighted gap faces.

The synthetic gap had a width of 6.20 mm and a flush of 0.30 mm. The results of measuring along the x- and y-axis are presented in Table 2. We observed that the measurements were very close to the real dimensions. The measured mean width values were between 6.21 and 6.22 with a standard deviation of 0.02–0.03 mm. The mean flush was measured between 0.28 and 0.33 mm with a standard deviation of 0.03–0.04 mm. The accuracy within the area of 80 mm $\times$ 80 mm was better than 0.1 mm and was almost the same for width and flush. Factors that influence adversely the measurements are the acquisition and spatial digitization noise, the errors in the line extraction and the inaccuracies of camera parameters (calibration error). The error measured in this experiment is the result of the combination of all the above factors.

At this point we should mention that the relative error of the flush measurement was quite big (25%). However, the relative error is actually not relevant for the assessment of a gap's quality. In the context of an inspection application we do not try to measure exactly the gap dimensions but to decide if they lie within some predefined limits. Therefore, only the absolute accuracy is important for measuring gaps [7–9].

3.2.2. Reference gap

In this experiment, we checked the accuracy of the measurement for both width and flush, using a reference gap (similar to the gaps of the manufactured vehicles). The LED lamps highlighted the gap faces, thus, producing bright lines. The overall error in this experiment is given by the superposition of the error in the vision system (estimated in Section 3.2.1) and the error due to the reflections, which is estimated by Eqs. (16a) and (16b). We used the same system configuration and the same procedure as in the previous section.

The width of the gap was 3.5 mm and the flush was 1 mm. The Eqs. (11a) and (11b) predicted a width-offset of 2.8 mm, thus, the expected width

Table 2
The width and flush measurement for displacement of the synthetic gap along the x- and y-axis

		Width (mm), actual: 6.20			Flush (mm), actual: 0.30		
		Mean	RMS error	Maximum error	Mean	RMS error	Maximum error
x	−20 to 20 mm	6.21	0.02	0.06	0.28	0.03	0.07
	−40 to 40 mm	6.22	0.04	0.07	0.28	0.04	0.07
y	−20 to 20 mm	6.22	0.02	0.05	0.31	0.03	0.06
	−40 to 40 mm	6.22	0.03	0.05	0.33	0.04	0.06

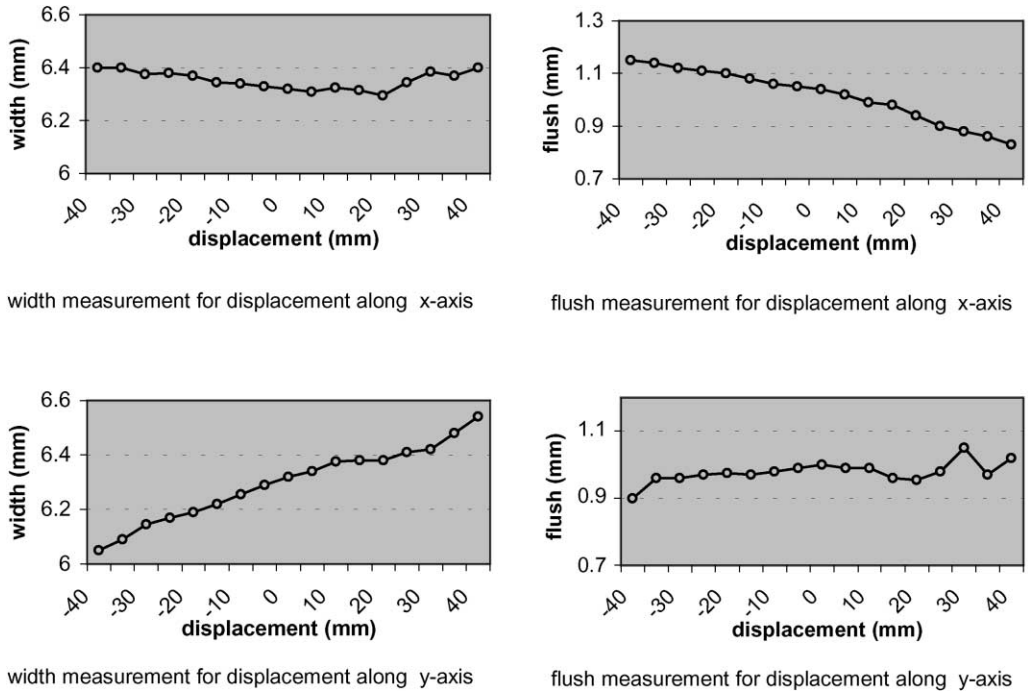

Fig. 8. Off-line measurements of the reference gap.

measurement was 6.3 mm. For flush the offset was calculated to be zero. The measurement results are presented in Fig. 8a–d and Table 3. The width was measured with an RMS (root mean square) error of 0.04 mm within an area of 40 mm × 40 mm and 0.13 mm within an area of 80 mm × 80 mm. For flush measurement the RMS error was 0.04 within an area of 40 mm × 40 mm and 0.10 mm within an area of 80 mm × 80 mm.

The results are consistent with the results of Section 2.3.2. The error in the width (flush) changes linearly as the gap is displaced along the *y*-axis (*x*-axis). The errors for the width (flush) along the *x*-axis (*y*-axis) have the almost the same behavior with those of the synthetic gap. The slopes that we obtain (Table 4) are close to those that we have theoretically calculated (Table 1). From the above we conclude that if we include in our system the Eqs. (16a) and (16b), the accuracy of the system will be improved drastically and in the ideal case only the error coming from the vision system will be present.

3.3. On-line test

In order to test the validity of our method under real conditions, we measured the gap between two doors

Table 3
The width and flush measurement, for displacement of the reference gap along the *x*- and *y*-axis

		Width (mm), actual + offset: 6.30			Flush (mm), actual + offset: 1.00		
		Mean	RMS error	Maximum error	Mean	RMS error	Maximum error
x	−20 to 20 mm	6.33	0.03	0.07	1.01	0.04	0.10
	−40 to 40 mm	6.36	0.06	0.10	1.03	0.10	0.17
y	−20 to 20 mm	6.37	0.04	0.11	0.98	0.02	0.05
	−40 to 40 mm	6.36	0.13	0.25	0.98	0.04	0.10

Table 4
The experimentally obtained slopes regarding the measurement of width and flush for displacement of the gap along the x- and the y-axis

Displacement of x-axis		Displacement of y-axis	
Width slope	Flush slope	Width slope	Flush slope
−0.00007	−0.00398	0.00541	0.00075

Table 5
Mean, root mean square and maximum error for measuring width and flush on-line

	Width (mm)	Flush (mm)
Mean error	0.07	0.08
RMS error	0.09	0.09
Maximum error	0.21	0.22

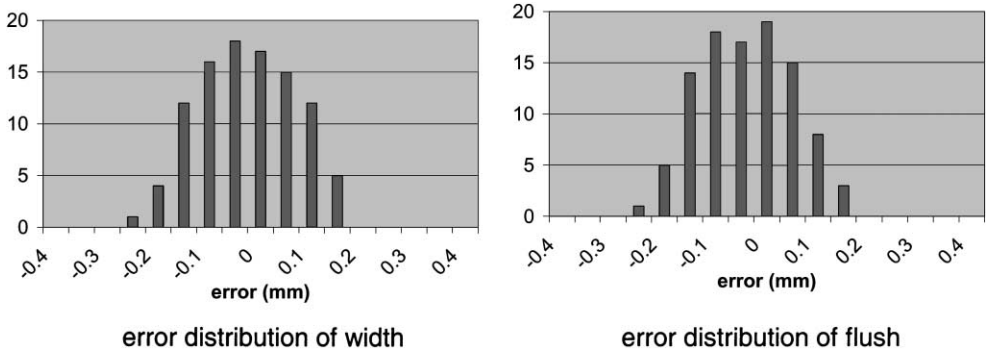

Fig. 9. The error distribution of width and flush for the on-line experiment.

on vehicles moving on the production line (on-line test). The measurement was executed for 100 cars. This experiment differs from the previous ones because the gap was displaced in both directions x and y simultaneously (± 20 mm). Furthermore, the measured vehicles covered the whole range of colors.

The installation that we used has been illustrated in Fig. 1. Every time a gap was in the cameras' field of view the light barrier sent a signal to the input–output card, which in turn switched on the lamps and triggered the vision software to grab and process three pairs of images. We used multiple exposures in order to improve the configuration's reliability (as reported by Fraser [23]). The conveyor speed was about 20 cm/s and resulted in a gap displacement of about 8 mm in x-axis between two consecutive exposures, which is within the aforementioned tolerances. The measurements were stored automatically. In this experiment, no a priori ground truth for the gap dimensions was available. We used as reference the measurements provided by an electronic gap-measuring device employing contact sensors (manufactured by Stankowitz GmbH). The resolution of this instrument is better than 0.1 mm. For the system measurements we used the correction factors given by the Eqs. (11a–b) and (16a–b). The error distribution is presented in Fig. 9. A 100% of the gaps were measured. The mean error was 0.07 mm for width, 0.08 for flush and the RMS error was 0.09 for both dimensions (see Table 5).

The above errors were expected since the vision system had an RMS error of 0.03 mm (as explained in Section 3.2.1). Moreover, the calculation of the correction factors is also subject to errors due to the approximations made as explained in Section 2.3.2. In addition, no ''ground truth'' was available for the gap dimensions.

4. Conclusions

A new method for measuring gaps has been introduced and demonstrated. We proved the feasibility of measuring the gap dimensions (width and flush) on colored cars, while moving on the assembly line, using specular reflection and stereo cameras. The RMS error of the measurement was <0.1 mm, which is very satisfactory for gap inspection.

The importance of such an application is obvious for the automobile industry. The gap-measuring task, so far executed by humans, has been time-consuming, inaccurate, insufficient and expensive. Our system measures quickly, accurately and consistently, independently of vehicle color and without mechanical contact. The whole gap-measuring procedure is automated, including the recording of information, thus, reducing significantly the costs and enabling constant monitoring of the production. Currently a prototype system operates on the assembly line of a major automobile manufacturer. The system consists of many pairs of cameras and lamps and is able to measure the most important gaps of a vehicle in <15 s. We should note that this prototype system measures in >30 positions and that the gaps are not measured simultaneously (due to hardware costs).

The system can be further improved by enhancing the image resolution, e.g. by using digital cameras. Since there are no real-time constraints the images can be processed off-line in order to cope with the increased processing requirements. A method for locating the lamps with higher accuracy would also contribute to better precision, because their position influences the calculation of the correction factors. We plan to investigate the applicability of the method in measuring gaps on transparent glass surfaces, since our preliminary experiments were promising (the laser methods are improper in that case). Furthermore, the system can be used to guide robots in fitting various panels on car bodies by employing gap measurement.

Acknowledgements

We wish to thank Dr. J. Schick, Mr. A. Dimopoulos and Dr. C. Tassakos for their useful comments as well as all the people who have assisted in the implementation of the software and the hardware of the system.

References

[1] J.D. Chalupnik, J.L. Garbini, J.E. Jorgensen, Shim Gap Gaging: A Survey of Applicable Technology, SME, Sensors 86, Detroit-Michigan, 1986.

[2] D.P. Sarr, T.W. Jurick, Faying surface gap measurement of aircraft structures for shim fabrication and installation, Proceedings SPIE Applications of Artificial Neural Networks II 1469 (1991) 506–514.

[3] W. Baudot, G. Clermont, P. Gaspart, P. Lococo, Visually guided arc-welding robot with self-training features, in: Proceedings of the SME 13th ISIR/Robots 7 Conference, Chicago, IL, 1983.

[4] O. Kropla, A sensor system for quality assurance in laser welding with filler wire, SPIE Laser Materials Processing and Machining 2246 (1994) 188–197.

[5] G.L. Oomen, W.J.P.A. Verbeek, A real-time optical profile sensor for robot arc welding, in: Proceedings of the 3rd International Conference on Robot Vision and Sensory Controls, Cambridge, MA, USA, November 1983.

[6] G. Pritschow, A. Horn, Schnelle adaptive signalverarbeitung für lichtsensoren, Robotersysteme 7 (1991) 193–203.

[7] Third Dimension Software Ltd., Gap Gun, 1999, http://www.third.com/GapGun.

[8] Oxford Sensor Technology Ltd., QuickScan Profile Measurement Sensor, 1999 http://www.oxfordsensors.com/products/css4.html.

[9] Oxford Sensor Technology Ltd., 1999, Specular Reflection Sensor, http://www.oxfordsensors.com/products/srs2.html.

[10] S.T. Barnard, M.A. Fischler, Computational stereo, ACM Computing Surveys 14 (4) (1982) 553–572.

[11] D.N. Bhat, S.K. Nayar, Stereo and specular reflection, International Journal of Computer Vision 26 (2) (1998) 91–106.

[12] M. Oren, S.K. Nayar, Theory of specular surface geometry, International Journal of Computer Vision 24 (2) (1996) 105–124.

[13] J.J. Koenderink, A.J. van Doorn, Photometric invariants related to solid shapes, Optica Acta 27 (7) (1980) 981–996.

[14] K.A. Tarabanis, P.K. Allen, R.Y. Tsai, A survey of sensor planning in computer vision, IEEE Transactions on Robotics and Automation 11 (1) (1995) 86–104.

[15] C.K. Cowan, P.D. Kovesi, Automatic sensor placement from vision task requirements, IEEE Transactions on Pattern Analysis and Machine Intelligence 10 (3) (1988) 407–416.

[16] S.O. Mason, A. Grün, Automatic sensor placement for accurate dimensional inspection, Computer Vision and Image Understanding 61 (3) (1995) 454–467.

[17] K.A. Tarabanis, R.Y. Tsai, P.K. Allen, The MVP sensor planning system for robotic vision tasks, IEEE Transactions on Robotics and Automation 11 (1) (1995) 72–85.

[18] M. Kass, A. Witkin, D. Terzopoulos, Snakes: active contours models, International Journal of Computer Vision 1 (4) (1988) 321–331.

[19] K.F. Lai, Deformable Contours: Modelling, Extraction, Detection and Classification, Ph.D. Thesis, University of Wisconsin, Madison, 1994.

[20] R.Y. Tsai, A versatile camera calibration technique for high-accuracy 3D machine vision metrology using off-the-shelf TV cameras and lenses, IEEE Journal of Robotics and Automation 3 (4) (1987) 323–344.

[21] R.K. Lenz, R.Y. Tsai, Techniques for calibration of the scale factor and image center for high accuracy 3D machine vision

metrology, IEEE Transactions on Pattern Analysis and Machine Intelligence 10 (10) (1992) 123–151.

[22] G.D. Hager, A modular system for robust positioning using feedback from stereo vision, IEEE Transactions on Robotics and Automation 13 (4) (1997) 582–595.

[23] C.S. Fraser, Network design considerations for non-topographic photogrammetry, Photogrammetric Engineering and Remote Sensing 50 (8) (1984) 1115–1126.